Submitted to Scripta Materialia in revised form, March 2019

Effect of nanometric γ′-particles on the stress-induced martensitic transformation in ⟨001⟩-oriented $Co_{49}Ni_{21}Ga_{30}$ shape memory alloy single crystals

C. Lauhoff[1*], A. Reul[2], D. Langenkämper[3], P. Krooß[1], C. Somsen[3], M.J. Gutmann[4], I. Kireeva[5], Y.I. Chumlyakov[5], W.W. Schmahl[2], T. Niendorf[1]

[1] *Institut für Werkstofftechnik (Materials Engineering), Universität Kassel, 34125 Kassel, Germany*
[2] *Applied Crystallography, Department of Earth and Environmental Sciences, Ludwig-Maximilians-Universität, 80333 Munich, Germany*
[3] *Institut für Werkstoffe, Ruhr-Universität Bochum, 44801 Bochum, Germany*
[4] *ISIS Facility, Rutherford Appleton Laboratory, Chilton, Didcot, Oxfordshire OX11 0QX, UK*
[5] *Siberian Physical Technical Institute, Tomsk State University, Novosobornay Square 1, 634050 Tomsk, Russia*

The effect of finely dispersed particles on the functional properties and morphology of thermally induced martensite in Co-Ni-Ga shape memory alloys has been already reported in literature, however, still important aspects are not fully understood. The current study focuses on the stress-induced martensitic transformation of solution-annealed, i.e. precipitate-free, and aged ⟨001⟩-oriented single crystals. *In situ* optical microscopy and neutron diffraction experiments show a significant influence of γ′-particles on the martensite variant selection and its morphology under pseudoelastic deformation. In addition, the results reveal detwinning upon loading in the presence of nanometric particles, which is experimentally proven for the first time.

Keywords: Shape memory alloys (SMAs), martensitic phase transformation, nanometric particles, neutron diffraction, Co-Ni-Ga

Over the last decades lots of research efforts have been made to obtain high-temperature pseudoelasticity (PE) and/or shape memory effect (SME) in shape memory alloys (SMAs) in order to overcome the application temperature limitations of the well-known binary Ni-Ti SMAs [1,2]. The addition of third elements to Ni-Ti [3–6] is a common practice to increase martensite start temperatures (M_s). Furthermore, precipitation hardening is an effective and well-established method to obtain high-temperature PE by increasing the strength of the parent austenitic phase [1,2]. However, besides strengthening of the matrix by precipitations, functional properties such as temperatures and hysteresis of the martensitic transformation (MT) as well as microstructure of the martensite are affected as well [2,7]. In particular, fine dispersions of nanometric particles with sizes up to tens of nm are of special interest due to their distinct impact on the functional properties in both, conventional SMAs, e.g. Ni-Ti [8,9], Cu-Zn-Al [10] and Fe-based alloys [11–13] as well as HT-SMA systems [1].

The Heusler type Co-Ni-Ga alloys undergo a thermoelastic MT from a cubic B2-ordered austenite to a tetragonal $L1_0$ martensite [14,15]. These alloys have gained significant attention due to their high potential for high-temperature applications owing to their excellent functional properties at elevated temperatures and relatively good formability induced by the γ-phase (A1) [16–22]. In two very recent studies a novel thermo-mechanical processing route based on hot extrusion was established allowing robust processing of Co-Ni-Ga. Good shape memory properties were obtained through process-induced formation of an oligocrystalline microstructure [23,24]. In addition to microstructure, phase transformation temperatures can be tailored in Co-Ni-Ga through aging of martensite referred to as SIM-aging [25,26]. In the austenitic phase, low and intermediate temperature heat treatments promote precipitation of the ordered γ′-phase ($L1_2$), which significantly increases the hardness of the matrix [21,27]. *In situ*

scanning electron microscopy (SEM) analysis upon cooling revealed a strong dependence of the microstructure of thermally induced martensite on size and morphology of γ′-particles [27,28]. In case of pseudoelastic testing a more complex and multi-variant microstructure is supposed to dominate the stress-induced martensite transformation (SIMT) [29]. Up to now, no studies are available in literature showing detailed microstructural investigations identifying the influence of γ′-particles on the SIMT, martensite variant selection and martensite morphology, respectively. Dadda et al. [16,17,30] only analyzed the complex microstructure evolution during SIMT as affected by temperature and training procedures in as-grown Co-Ni-Ga single crystals. The present study focuses on the SIMT of a near-⟨001⟩-oriented $Co_{49}Ni_{21}Ga_{30}$ single crystal (for better readability ⟨001⟩-oriented in the remainder of the text) in solution-annealed, i.e. precipitate-free, and aged condition. *In situ* optical microscopy (OM) as well as neutron diffraction were carried out at different stages of PE experiments. Fundamental differences in microstructure evolution were found and interrelationships between finely dispersed particles and the MT are established.

Ingots of Co-Ni-Ga with a nominal composition of 49Co-21Ni-30Ga (in at.%) were produced using vacuum induction melting. Single crystals were grown by Bridgeman technique in a He environment. For compression tests a single specimen with geometry of $4\times4\times8mm^3$ was used, which was electro-discharge machined (EDM) from one of the bulk single crystals such that the longer (i.e. loading) axis was parallel to the ⟨001⟩ crystal direction of the austenite (cf. Figure 2) while the lateral surfaces were ⟨100⟩ and ⟨010⟩. The specimen was mechanically ground down to remove the EDM affected surface layer. In order to investigate the influence of nanometric particles on the MT, the specimen was tested in both, solution-annealed and aged condition, i.e. containing γ′-particles. For solution-annealing the specimen was encapsulated in quartz glass

tubes under argon atmosphere and subsequently solution-annealed at 1200°C for 12h following air cooling. The aging was performed at 350°C for 1h under ambient atmosphere. Aging parameters were chosen in accordance to Refs. [27,28], both studies detailing the impact of the precipitates established by this heat treatment on the thermally induced martensitic transformation.

Quasi-static uniaxial single cycle compression experiments were conducted at 100°C on a servohydraulic test frame in displacement control at a nominal strain rate of $1\times10^{-3}s^{-1}$ up to a maximum strain of -5% upon loading and a minimum load of -200N for unloading. The selected test temperature ensured a fully austenitic state before pseudoelastic testing of both conditions. Strains were measured using a high-temperature extensometer with a gauge length of 12 mm directly attached to the grips. For calculation of the nominal strain the grips were treated as absolutely rigid. Heating of the specimen to the test temperature was achieved by controlled convection furnaces. Temperatures were measured via a thermocouple directly attached to the sample surface by a steel spring. *In situ* OM analysis was performed at various stages of the pseudoelastic stress-strain hysteresis. Surface images of the transforming specimen were captured using a digital microscope equipped with a tele-zoom objective. A representative surface area of about $3.5\times2.5mm^2$ was characterized. In addition to the standard mechanical grinding down to 5µm grit size, one of the side surfaces was mechanically polished with a 0.05µm polishing suspension. All grinding and polishing procedures of the specimen were performed in the austenitic state.

In situ neutron diffraction was carried out using the single crystal diffractometer SXD [31] at the ISIS neutron source, Oxfordshire. Uniaxial compression tests were performed using a miniature load frame under the same conditions as in the *in situ* OM experiment. Diffraction

data were recorded during each loading stage in the austenitic and martensitic state for 20 and 130min, respectively. Displacement at each loading stage was calibrated from stress values from the *in situ* OM experiment. For further details on the setup of SXD the reader is referred to [31,32].

Microstructural characterization of the γ′-particles was conducted using a transmission electron microscope (TEM) operating at a nominal voltage of 200kV. For TEM work, small discs were cut perpendicular to the ⟨001⟩ crystal direction of the austenite. For further details on TEM sample preparation the reader is referred to [26].

Upon solution-annealing at 1200°C, Co-Ni-Ga single crystals feature a single phase microstructure, as proven by TEM (not shown). Aging treatments at relatively low temperatures are effective for the formation of finely dispersed coherent second phase precipitates in the austenitic matrix [27,28]. After aging at 350°C for 1h, selected area diffraction (SAED) patterns (Fig. 1a) obtained from the $[001]_{B2}$ zone axis reveal reflections attributed to the γ′-phase (marked by the white arrows in Fig. 1a). The γ′-particles ($L1_2$, as revealed by the fast Fourier transformation (FFT) pattern (inset in Fig. 1b)) feature a spheroidal shape with diameters up to 5 nm, which is in good agreement to other studies [27,28].

Fig. 2 shows the compressive pseudoelastic response at 100°C of the ⟨001⟩-oriented $Co_{49}Ni_{21}Ga_{30}$ single crystalline specimen in solution-annealed as well as aged condition, respectively. Both conditions demonstrate excellent PE revealing fully reversible MT. The solution-annealed condition is characterized by a low critical stress σ_{cr} for MT of about 160MPa, a narrow stress hysteresis $\Delta\sigma$ of 30MPa, a transformation strain ε_{tr} of -4.2% and a plateau-type character of the forward transformation. These functional properties are in excellent agreement with the pseudoelastic behavior being already reported for solution-annealed [26] and as-grown

[16,33] Co-Ni-Ga single crystals. The subsequent aging treatment leads to the formation of finely dispersed γ′-precipitates (Fig. 1) and causes a substantially different stress-strain response, i.e. an increase of both, σ_{cr} and $\Delta\sigma$, a decrease of ε_{tr} as well as strain-hardening during forward transformation (Fig. 2).

In general, the underlying microstructural mechanisms responsible for these differences are reported in literature [27–29,34,35]. Three terms additively contribute to the increased value of $\sigma_{cr,}$ imposed by a change in the chemical and non-chemical contributions of the Gibbs free energy: The nanometric γ′-particles cause a change in the chemical composition of the matrix, an increase of the elastic energy accumulated during MT, and an increase of the irreversible energy dissipation. The last term mainly results from increased frictional work during interfacial motion and dissipation of high interfacial energy. Even if not experimentally proven, it has been suggested that this type of energy dissipation during pseudoelastic loading is induced by complexly accommodated martensite in the vicinity of the precipitates. So far, this was only shown for thermally induced $L1_0$ martensite [28,29]. In fact, a complex multi-variant accommodation of martensite lowers the transformation strain and is decisive for the stress-hardening and the increased hysteresis values [28–30]. However, in order to shed light on these elementary microstructural mechanisms, the influence of the γ′-phase on stress-induced martensite will be presented and discussed in the following focusing on the martensite variant selection and morphology.

Expectedly, the presence of γ′-particles strongly affects the SIMT, as evidenced by the *in situ* OM analysis. Fig. 3 shows micrographs that were recorded for the solution-annealed (Fig. 3a, b) and aged (Fig. 3c,d) condition at -3% and -5% strain upon loading, respectively. The reference austenitic microstructure of the specimen taken before testing is shown in the inset of

Fig. 2. For the sake of brevity, this study focuses only on the forward MT. However, work is already in progress analyzing the back transformation as well. In terms of the solution-annealed condition, the micrograph shown in Fig. 3a reveals a lamellar martensitic microstructure with a dominant martensite plate (top right corner) and a few additional smaller ones coexisting with the untransformed austenite (A) at -3% strain. Martensite plates separated by a direct interface to austenite are termed habit plane variants (HPVs) in the following, and each martensite plate comprises two twin-related domain variants [32,36], referred to as correspondent variant pair (CVP). The HPVs in Fig. 3a featuring the same crystallographic orientation with respect to the loading direction, consist of the same CVP, referred to as CVP_1. Following straining of the specimen to -5% (Fig. 3b), the MT is fully accomplished without the formation of differently oriented HPVs. In consequence, the MT of the solution-annealed single phase condition is characterized by the formation of a single (internally twinned) variant of stress-induced martensite, i.e. CVP_1 (Fig 3a,b). This heterogeneous transformation behavior [30] is in excellent agreement with as-grown ⟨001⟩-oriented $Co_{49}Ni_{21}Ga_{30}$ single crystals [30,32]. The narrow stress hysteresis and plateau-type character of the forward transformation (Fig. 2) can be explained by the growth of this single CVP. Due to low interfacial friction, phase fronts can easily move during the SIMT [16,17].

As revealed by the optical micrographs in Fig. 3c,d, precipitation of nanometric γ′-particles affects the martensite variant selection and the morphology of the stress-induced martensite. In addition to the initial CVP_1 (Fig. 3a,b), the forward transformation of the aged condition is characterized by evolution of HPVs of a second orientation with respect to the loading direction (both orientations are marked by dashed lines in Fig. 3c). Furthermore, the phase transformation proceeds by simultaneous formation of numerous interfaces. In contrast to the well-defined

habit planes prevailing during the MT in the solution-annealed condition (Fig. 3a), pronounced interactions among these various moving phase boundaries lead to local evolution of distorted interfaces. This phenomenon is observed especially when HPVs of different orientations interact with each other. This complex self-accommodated type of martensite configuration being indicative for a quasi-homogenous MT behavior in SMAs [37], impedes a reliable identification of the number of variants. Hence, bulk data obtained by neutron diffraction experiments were used to shed light on the martensite variant selection. For this purpose, the specimen in the aged condition, which already was probed in the *in situ* OM analysis (Fig. 2 and 3c,d), was investigated in a subsequent *in situ* neutron diffraction experiment at 100°C at the ISIS neutron source. The diffractograms shown in Fig. 4 correspond to the unloaded, entirely austenitic state before testing (Fig. 4a) and to states upon applying strains of -3% (Fig. 4b) and -5% (Fig. 4c), respectively. The diffractogram at -3% strain shows an austenite reflection (A) in between four martensite domain variant reflections (V_1–V_4) confirming the aforementioned observations. The formation of habit planes under load leads to a slight misorientation between different austenitic parts of the sample as indicated by vertical splitting of the austenite reflection. Precipitation of finely dispersed γ′-particles causes the formation of two differently internally twinned types of HPVs, i.e. CVP_1 and CVP_2. Based on analysis of the diffraction spots, the martensite domain variants V_1/V_2 and V_3/V_4 each form a CVP, respectively. Upon loading to -5% strain the formation of stress-induced martensite is completed as indicated by the annihilated reflection of austenite. Furthermore, additional domain variants were not detected as seen in the corresponding diffractogram. However, the optical micrograph at -5% indicates partial detwinning in strip-like structures [36], which are oriented nearly parallel to the loading direction (marked by the black arrow in Fig. 3d). Martensite detwinning of internally

twinned CVPs is induced by growth of one of the domain variants within a CVP via twin-boundary motion. By analyzing the diffraction intensities as a function of the applied compressive strain (Fig. 4d) the detwinning process upon loading can be further substantiated. The intensity ratios V_1/V_2 and V_3/V_4 change upon straining from -3% to -5%, clearly indicating an increase of volume fraction of one of the domain variants at the expense of the other one, i.e. detwinning. Even though only partial detwinning is observed, this is not expected for the ⟨001⟩ direction under compressive loading in Co-Ni-Ga based on theoretical calculations [17]. Furthermore, nanometric particles have been reported to hamper the detwinning process [29]. Thus, the role of precipitates in SMAs needs to be reconsidered carefully, as new high-performance applications of precipitation-hardened alloy systems are potentially enabled due to additional detwinning strains. Indeed, further work is needed to reveal the full potential of differently designed precipitates on the detwinning mechanisms.

Besides these observations for Co-Ni-Ga other microstructural factors can lead to a multi-variant martensite selection. Dadda et al. [16,30] demonstrated the presence of a multi-variant self-accommodated martensite morphology upon SIMT owing to diffusion of point defects and kinetic pinning-induced martensite stabilization [38] at elevated temperatures above 120°C [30,38]. This mechanism is negligible here due to the lower test temperature of 100°C as can be deduced from the heterogeneous transformation behavior of the solution-annealed condition (Fig. 2). In the present study, the complex martensite microstructure of the aged condition results from coherency stress fields imposed by the nanometric precipitates [8,9]. Unlike CVP_1, which is favored by the external applied stress, the formation of CVP_2 is obviously promoted due to its favorable orientation to the stress fields existing around the γ′-particles [8,29,39]. In addition, the refinement of the $L1_0$ martensite (formation of numerous interfaces during stress-

induced MT (Fig. 3c)) results from both, difficulties in shaping the martensite within the irregular stress fields around the particles and an increase in elastic energy accumulation owing to significant elastic deformation of the non-transforming particles and the surrounding matrix [28,29]. Such a microstructure with pronounced variant-variant interactions is the origin of irreversible processes during SIMT contributing to the different stress-strain response in terms of the stress hysteresis, stress hardening and transformation strain in comparison to the single phase condition (Fig. 2). The increased stress hysteresis is also induced by the observed detwinning process, which is known to promote mechanical stabilization of martensite [40]. Further clarification is needed regarding cyclic stability and fatigue life, not only for precipitation-hardened Co-Ni-Ga SMAs, but also in other SMAs, e.g. iron-based SMAs, in which the presence of particles is a prerequisite for a thermoelastic MT [11,41].

In conclusion, fundamentally different martensitic transformation (MT) behaviors for a ⟨001⟩-oriented $Co_{49}Ni_{21}Ga_{30}$ single crystal in solution-annealed and aged condition were verified by *in situ* experiments. Whereas a single, internally twinned martensite is present in the precipitate-free condition, nanometric γ′-particles lead to a self-accommodated martensite morphology featuring two CVPs. In addition, bulk information obtained by neutron diffraction reveals a detwinning process, which has not been revealed for ⟨001⟩-oriented $Co_{49}Ni_{21}Ga_{30}$ single crystals before.

This work was supported by Deutsche Forschungsgemeinschaft (DFG) within the Research Unit Program “Hochtemperatur-Formgedächtnislegierungen” (Contract nos. NI1327/3-2; SCHM930/13-2; SO505/2-2); and the Ministry of Science and Education of Russian Federation (State Task no. 16.6554.2017/6.7). The authors gratefully acknowledge the assistance of Keith

Allum (ISIS neutron source, Oxfordshire), Bjoern Pedersen (FRM II research neutron source, Garching), Thomas Pham and Michael Wiegand with the experiments.

References

[1] J. Ma, I. Karaman, R.D. Noebe, Int. Mater. Rev. 55 (2013) 257.
[2] K. Otsuka (Ed.), Shape memory materials, 1st ed., Cambridge Univ. Press, Cambridge, 1999.
[3] G.S. Firstov, J. van Humbeeck, Y.N. Koval, Mater. Sci. Eng., A 378 (2004) 2.
[4] K. Otsuka, X. Ren, Prog. Mater Sci. 50 (2005) 511.
[5] H. Sehitoglu, L. Patriarca, Y. Wu, Curr. Opin. Solid State Mater. Sci. 21 (2017) 113.
[6] K.P. Mohanchandra, D. Shin, G.P. Carman, Smart Mater. Struct. 14 (2005) S312-S316.
[7] D.C. Lagoudas, Shape memory alloys: Modeling and engineering applications, Springer, Boston, MA, 2008.
[8] K. Gall, H. Sehitoglu, Trans. ASME 121 (1999) 19.
[9] K. Gall, H. Sehitoglu, Trans. ASME 121 (1999) 28.
[10] F.d.C. Bubani, F.C. Lovey, M.L. Sade, Funct. Mater. Lett. 10 (2017) 1740006.
[11] Y. Tanaka, Y. Himuro, R. Kainuma, Y. Sutou, T. Omori, K. Ishida, Science 327 (2010) 1488.
[12] J. Ma, B.C. Hornbuckle, I. Karaman, G.B. Thompson, Z.P. Luo, Y.I. Chumlyakov, Acta Mater. 61 (2013) 3445.
[13] Y.I. Chumlyakov, I.V. Kireeva, O.A. Kutz, A.S. Turabi, H.E. Karaca, I. Karaman, Scr. Mater. 119 (2016) 43.
[14] M. Wuttig, J. Li, C. Craciunescu, Scr. Mater. 44 (2001) 2393.
[15] K. Oikawa, T. Ota, F. Gejima, T. Ohmori, R. Kainuma, K. Ishida, Mater. Trans. 42 (2001) 2472.
[16] J. Dadda, H.J. Maier, I. Karaman, H.E. Karaca, Y.I. Chumlyakov, Scr. Mater. 55 (2006) 663.
[17] J. Dadda, H.J. Maier, D. Niklasch, I. Karaman, H.E. Karaca, Y.I. Chumlyakov, Metall. Mater. Trans. A 39 (2008) 2026.
[18] P. Krooß, P.M. Kadletz, C. Somsen, M.J. Gutmann, Y.I. Chumlyakov, W.W. Schmahl, H.J. Maier, T. Niendorf, Shap. Mem. Superelasticity 2 (2016) 37.
[19] P. Krooß, T. Niendorf, P.M. Kadletz, C. Somsen, M.J. Gutmann, Y.I. Chumlyakov, W.W. Schmahl, G. Eggeler, H.J. Maier, Shap. Mem. Superelasticity 1 (2015) 6.
[20] J. Liu, H. Xie, Y. Huo, H. Zheng, J. Li, J. Alloys Compd. 420 (2006) 145.
[21] E. Dogan, I. Karaman, Y.I. Chumlyakov, Z.P. Luo, Acta Mater. 59 (2011) 1168.
[22] M. Vollmer, P. Krooß, C. Segel, A. Weidner, A. Paulsen, J. Frenzel, M. Schaper, G. Eggeler, H.J. Maier, T. Niendorf, J. Alloys Compd. 633 (2015) 288.
[23] T. Niendorf, C. Lauhoff, E. Karsten, G. Gerstein, A. Liehr, P. Krooß, H.J. Maier, Scr. Mater. 162 (2019) 127.

[24] E. Karsten, G. Gerstein, O. Golovko, A. Dalinger, C. Lauhoff, P. Krooss, T. Niendorf, A. Samsonenko, H.J. Maier, Shap. Mem. Superelasticity 50 (2019) 511.
[25] C. Lauhoff, P. Krooß, D. Langenkämper, C. Somsen, G. Eggeler, I. Kireeva, Y.I. Chumlyakov, T. Niendorf, Funct. Mater. Lett. 11 (2018) 1850024.
[26] T. Niendorf, P. Krooß, C. Somsen, G. Eggeler, Y.I. Chumlyakov, H.J. Maier, Acta Mater. 89 (2015) 298.
[27] Y.I. Chumlyakov, I.V. Kireeva, E.Y. Panchenko, V.A. Kirillov, E.E. Timofeeva, I.V. Kretinina, Y.N. Danil'son, I. Karaman, H. Maier, E. Cesari, Russ. Phys. J. 54 (2012) 937.
[28] I.V. Kireeva, J. Pons, C. Picornell, Y.I. Chumlyakov, E. Cesari, I.V. Kretinina, Intermetallic. 35 (2013) 60.
[29] I.V. Kireeva, C. Picornell, J. Pons, I.V. Kretinina, Y.I. Chumlyakov, E. Cesari, Acta Mater. 68 (2014) 127.
[30] J. Dadda, H. J-rgen Maier, I. Karaman, Y. Chumlyakov, Int. J. Mater. Res. 101 (2010) 1.
[31] D.A. Keen, M.J. Gutmann, C.C. Wilson, J. Appl. Crystallogr. 39 (2006) 714.
[32] A. Reul, C. Lauhoff, P. Krooß, M.J. Gutmann, P.M. Kadletz, Y.I. Chumlyakov, T. Niendorf, W.W. Schmahl, Shap. Mem. Superelasticity 21 (2018) 113.
[33] I.V. Kireeva, Z.V. Pobedennaya, Y.I. Chumlyakov, J. Pons, E. Cesari, I. Karaman, Tech. Phys. Lett. 35 (2009) 186.
[34] I.V. Kretinina, O.A. Kuts, D.A. Kuksgauzen, V.V. Poklonov, Z.V. Pobedennaya, Y.N. Platonova, IOP Conf. Ser.: Mater. Sci. Eng. 71 (2015) 12061.
[35] G. Gerstein, V.A. L'vov, A. Kosogor, H.J. Maier, Mater. Lett. 210 (2018) 252.
[36] D. Niklasch, J. Dadda, H.J. Maier, I. Karaman, J. Mater. Sci. 43 (2008) 6890.
[37] J. Shaw, J. Mech. Phys. Solids 43 (1995) 1243.
[38] S. Kustov, J. Pons, E. Cesari, J. van Humbeeck, Acta Mater. 52 (2004) 3083.
[39] R.F. Hamilton, H. Sehitoglu, Y. Chumlyakov, H.J. Maier, Acta Mater. 52 (2004) 3383.
[40] V.A. Chernenko, J. Pons, E. Cesari, I.K. Zasimchuk, Scr. Mater. 50 (2004) 225.
[41] P. Krooß, C. Somsen, T. Niendorf, M. Schaper, I. Karaman, Y. Chumlyakov, G. Eggeler, H.J. Maier, Acta Mater. 79 (2014) 126.

Figure 1

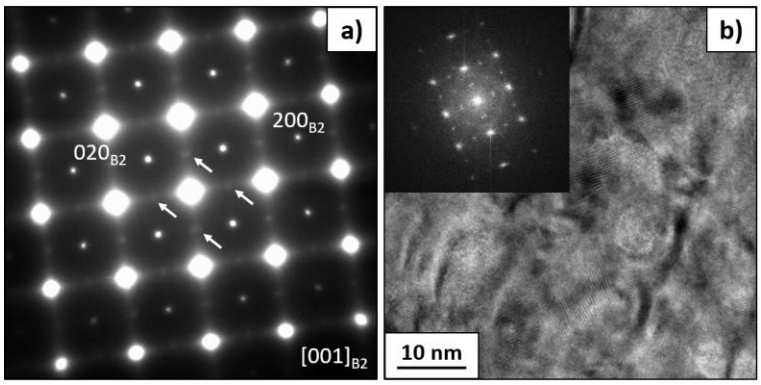

Figure 1: TEM analysis of the $Co_{49}Ni_{21}Ga_{30}$ alloy following solution-annealing and aging at 350°C for 1h. (a) SAED pattern with diffuse superlattice reflection spots of the γ'-phase marked by the white arrows. (b) HRTEM image of γ'-particles formed after aging. The inset shows the corresponding FFT pattern obtained in the $[001]_{B2}$ zone axis.

Figure 2

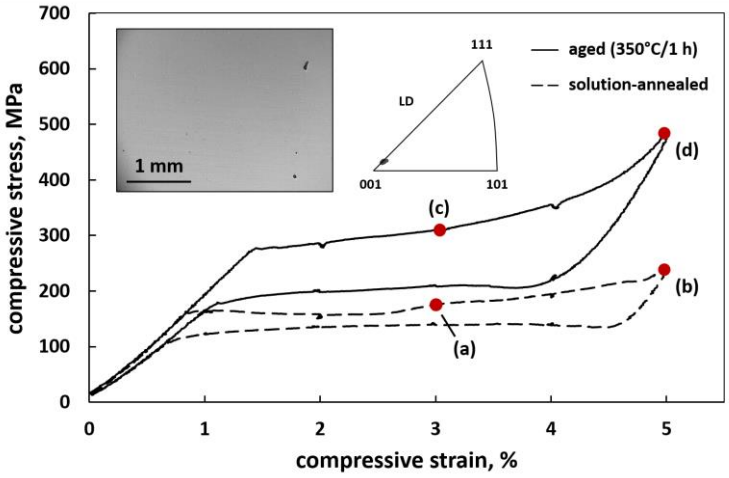

Figure 2: Stress-strain curves of a ⟨001⟩-oriented $Co_{49}Ni_{21}Ga_{30}$ crystal, solution-annealed (lower hysteresis) and subsequently aged (upper hysteresis), under compressive load at 100°C. The optical micrograph and the inverse pole figure in the inset show the reference austenitic microstructure of the specimen taken in the unloaded solution-annealed condition before testing and the orientation of the austenitic phase with respect to the loading direction (LD), respectively. The red points (a)-(d) correspond to the optical micrographs shown in Fig. 3.

Figure 3

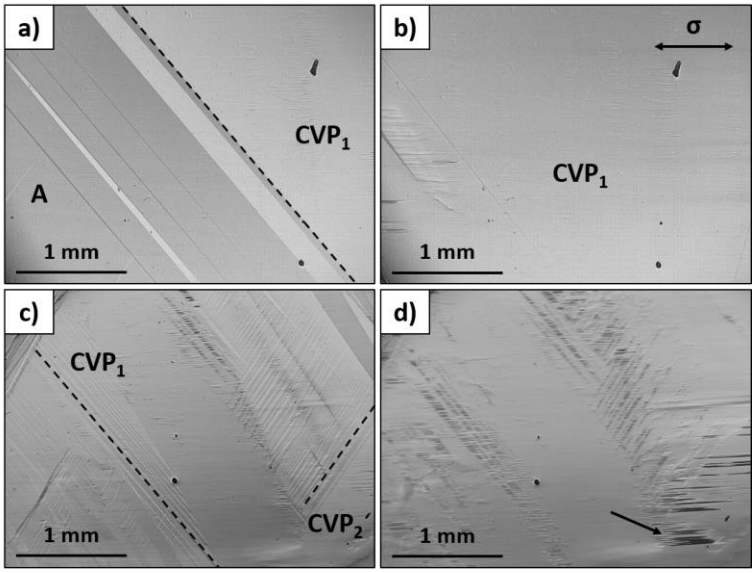

Figure 3: In situ OM analysis of the ⟨001⟩-oriented $Co_{49}Ni_{21}Ga_{30}$ specimen in the solution-annealed (a,b) and aged (c,d) condition under compression at 100°C. The micrographs show a lateral ⟨100⟩ sur*face and were recorded at the marked positions of the stress-strain curves in Fig. 2, i.e. (a,c) and (b,d) at -3 % and -5 % strain, respectively. Loading direction is marked in the upper right corner of image (b). See main text for details.*

Figure 4

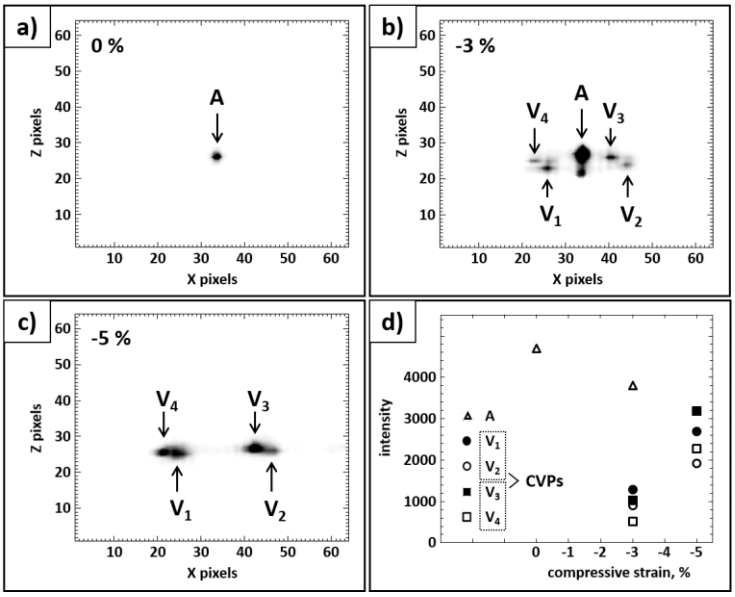

Figure 4: In situ neutron diffraction analysis of the ⟨001⟩-oriented $Co_{49}Ni_{21}Ga_{30}$ specimen in the aged condition during a pseudoelastic single cycle experiment under compressive load at 100°C. Diffractograms (a-c) were obtained in load-free state as well as upon -3% and -5% of strain. The diffraction intensity plotted as a function of compressive strain is illustrated in (d).